Elastoplastic Discretized Virtual Internal Bond Model and Its Application to Dynamic Fracture Simulation in Rock

Dina Kon[1][(✉)], Alphonse Kakanda[2], Dave Mbako[2], and Shu Jisen[3]

[1] School of Mines, China University of Mining & Technology, Xuzhou, Jiangsu, China
dinakon25@gmail.com
[2] School of Naval Architecture, Ocean and Civil Engineering, Shanghai Jiao Tong University, Shanghai, China
[3] State Key Laboratory of Resources and Mine Safety, China University of Mining & Technology, Xuzhou, Jiangsu, China

Abstract. Failure of a material is always accompanied by plastic deformation and fracturing processes. Continuum plastic mechanics can handle plastic deformation effectively when it employs a yield function and the flow rule. As a result of its inability to account for the microstructure of the material, the continuum mechanics method has some drawbacks when addressing the fracture problem. The lattice model can simulate the fracture problem quite well, but it is insufficient for plastic deformation. The aim of this paper is to embed the modified Stillinger-Weber potential in the discretized virtual internal bond (SW-DVIB) in order to simulate the plastic deformation and fracture at the bond level. In the original DVIB, the interaction between particles in a cell is characterized by an interatomic bond potential, which intrinsically contains the microfracture mechanism. Nevertheless, because the interatomic potential only accounts for the effect of the bond stretch, the Poisson ratio it represents is fixed. To remedy this drawback, the plasticity is embedded into the modified Stillinger-Weber potential, and the elastoplastic SW-DVIB is developed so that it can simulate the elastoplastic fracture and deformation in the solid with different Poisson ratios. The simulation results show that the method can simulate the fracture behaviors and the plastic deformation with accuracy because it is based on the discrete lattice structure of the elastoplastic SW-DVIB and is efficient in dealing with the model-induced fracture propagation problem.

Keywords: Plastic deformation · lattice model · plastic fracture · modified Stillinger-Weber potential · discretized virtual internal bond

1 Introduction

The continuum mechanics method can be used to simulate elastoplastic fracture, but its limitation lies in the lack of considering mesostructural characteristics of the material in the constitutive relationship; meanwhile, micro- and meso-models established at the

atomic and molecular levels are limited by computational limitations to small-scale simulations. To overcome such limitations, some scholars proposed a quasi-continuous medium method, which can be traced back to the quasi-continuous model proposed by Tadmor et al. [1, 2]. The quasi-continuous (QC) method is an approach used to construct macroscopic constitutive equations of a material using the interaction potential between atoms. The finite element method is employed to reduce the degrees of freedom, while judgment criteria are used to determine local and non-local atom energies. Shilkrot et al. [3, 4] have developed a plastic multi-scale model and an atomic-continuum coupled approach to simulate dislocations and two-scale interfaces respectively. The QC model is an effective way of reflecting the micro-mechanical structure of materials, but has the limitation of unbalanced "Ghost Force". Other methods, such as Coarse-Grained Molecular Dynamics (CGMD) [5] and Bridge Domain Scale (BS) [6, 7] have been proposed to deal with this issue. The Virtual Internal Bond (VIB) [8] model has also been used to simulate elastoplastic fracture, decomposing the strain into elastic and plastic parts, and using the two-body potential to characterize interactions between particles. To solve the problem of the Poisson ratio, the effect of bond rotation and bond angle was considered in the VIB model by Zhang and Ge [9]. The Finite Element Method (FEM) and Extended Finite Element Method (XFEM) [10] are powerful numerical analysis methods used to simulate material damage without needing to re-mesh in the process [11]. However, the linear elastic fracture mechanics used in these methods are not suitable for heterogeneous brittle materials like rock or concrete due to the presence of many micro-cracks [12]. This has led to the development of the Meshless Method and Statistical Strength Theory [13, 14], which approaches the problem of fracture propagation by analyzing the accumulation of micro-cracks. The discrete model is a widely used method for simulating the fracturing process of materials, where the material is represented by a discrete structure composed of spring, bar, or beam elements. Different discrete models have been developed, such as the lattice model [15, 16], spring model [17], a discrete Unit method [18], particle flow method [19], and discontinuous deformation analysis [20]. The lattice model is the most common of these and is traced back to Hrenníkoff [21]. It is used to solve classical elastic mechanics problems and simulates the initiation and evolution of micro-damage in the material by the successive failure of individual bar or spring units. However, it still has problems with parameter calibration and the force criterion used to damage the rod can't account for hyperelastic behavior. Recent developments in hybrid lattice methods have improved the lattice model and allowed it to be used to study granular materials, fiber materials, and composite materials [22–25]. The parameter calibration of lattice models is complicated for 3D cases, as the macro Poisson's ratio is fixed [26]. To solve this, a beam element can be used to allow for shear effects, and an angular spring to limit the change of the angle [27–29]. Recently, Zhang developed the DVIB model which is composed of virtual unit bond cells and can take any geometry [30]. This provides an alternative to using beams and angular springs. The Discrete Viscous Bond (DVIB) model is a lattice model which can simulate large deformation dynamic fracture problems without external fracture criterion. Xu et al. [31] have combined the continuum plastic theory with the lattice model to consider the plastic deformation directly on the micro bond level. Zapperi et al. [32], Seppala et al. [33], and Picallo et al. [34], have considered plasticity in the arbitrary fuse grid which is analogous

to the lattice structure. Ding et al. [35] have also accounted for plastic deformation in DVIB, while Zhang and Chen [36] have used the modified Stillinger–Weber (SW) potential to describe the total energy of a bond cell and overcome the limitation of the fixed Poisson ratio. So far the DVIB can account for plastic deformation but the Poisson ratio is fixed while the SW-DVIB can represent the various Poisson ratio but it cannot account for the plastic deformation. To further improve the DVIB model and make it capable of accounting for both the plastic deformation and the various Poisson ratio, the SW-DVIB is extended to the plastic case in this paper. The plastic deformation will be considered in the two-body interaction of the modified SW potential and keep the three-body interaction elastic. By this means, the SW-DVIB can account for the plastic deformation on one hand. On the other hand, it can represent the various Poisson ratio. Thus, such plastic SW-DVIB can be used to simulate the elastoplastic fracture problem and plastic deformation.

2   Background of SW-DVIB

The Stillinger-Weber (SW) potential proposed in [37] is a combination of two and three-body interactions, with bond energy dependent on the bond length and bond angle. Originally, it was employed to model the silicon material, with the ideal tetrahedral angle acting as the reference bond angle. Zhang et al. [36], modified the SW potential in 2014 by using the bond angle from the reference configuration as its reference angle, making it more applicable to other materials than silicon as it is shown below (see Fig. 1).

$$W = \frac{1}{2} \sum_{I=1}^{N(N-1)} \Phi_2(l_I) + \frac{1}{2} \sum_{I=1}^{N(N-1)} \sum_{J\neq 1}^{N-2} \Phi_3(l_I, l_J, \theta_{IJ}) \tag{1}$$

$$F_i = \frac{\partial W}{\partial u_i} = \frac{1}{2} \sum_{I}^{N(N-1)} \frac{\partial \Phi_2}{\partial l_I} \cdot \frac{\partial l_I}{\partial u_i} + \frac{1}{2} \sum_{I}^{N(N-1)} \sum_{J}^{N-2} \frac{\partial \Phi_3}{\partial \theta_{IJ}} \cdot \frac{\partial \theta_{IJ}}{\partial u_i} \tag{2}$$

$$K_{ij} = \frac{\partial^2 W}{\partial u_i \partial u_j} = \frac{1}{2} \sum_{I}^{N(N-1)} \left(\frac{\partial^2 \Phi_2}{\partial l_I^2} \cdot \frac{\partial l_I}{\partial u_j} \cdot \frac{\partial l_I}{\partial u_i} + \frac{\partial \Phi_2}{\partial r_I} \cdot \frac{\partial^2 l_I}{\partial u_i \partial u_j} \right)$$
$$+ \frac{1}{2} \sum_{I}^{N(N-1)} \sum_{J}^{N-2} \left(\frac{\partial^2 \Phi_3}{\partial \theta_{IJ}^2} \cdot \frac{\partial \theta_{IJ}}{\partial u_j} \cdot \frac{\partial \theta_{IJ}}{\partial u_i} + \frac{\partial \Phi_3}{\partial \theta_{IJ}} \cdot \frac{\partial^2 \theta_{IJ}}{\partial u_i \partial u_j} \right) \tag{3}$$

For a bond cell shown in Fig. 1, the total energy is shown in Eq. (1). The constitutive relation of a bond cell is derived as the following. The node force and stiffness matrix are shown in Eqs. (2) and (3) respectively. The two-body and three-body interaction in the linear elastoplastic SW-bond potential can be written as:

$$\Phi_2 = \frac{1}{2}A(l - l_0)^2, \ldots \Phi_3 = \frac{1}{2}\lambda(\theta_{IJ} - \theta_{IJ0}) \tag{4}$$
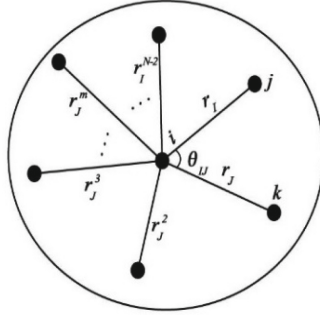
Fig. 1. A bond cell described by the modified SW potential

3 Consideration of Plasticity in SW-DVIB

The SW-potential includes two parts, namely the two-body and the three-body potential. To build up the elastoplastic SW-DVIB, the plasticity is considered in the two-body potential while the three-body potential is kept elastoplastic. So, the general constitutive relation of the SW-DVIB takes the form as shown in Eqs. (1). Ding et al. have considered the plasticity in the two-body potential of Eq. (2) [35]. In this new method, we consider the constitutive model of the elastoplastic SW-DVIB shown in [38]. In [39], the linear elastic-brittle three-body potential was developed. In the present elastoplastic SW-DVIB, this three-body potential is adopted:

$$
\Phi_3 = \begin{cases} \frac{1}{2}\lambda(\theta_{IJ} - \theta_{IJ0})^2 & \text{if } \max\left(\frac{l_I}{l_{I0}}, \frac{l_J}{l_{J0}}\right) \leq 1 + \varepsilon_r \text{ and } |\theta_{IJ} - \theta_{IJ0}| \leq \varepsilon_\theta \theta_{IJ0} \\ \quad\text{constant} & \text{else} \end{cases}
\tag{5}
$$

where ε_r is the critical bond length strain over which bond breaks; ε_θ is the critical bond angle strain over which bond angle loses its mechanical resistance. Ding et al. presented a diagram of the two-body potential, which was derived from the interpretation of the physical parameters [35]. To facilitate the parameter analysis, the dimensionless parameters defined in [35] are still used. The elastoplastic SW-DVIB parameters were calibrated using the methodology proposed by Zhang [39].

$$
\begin{aligned}
k_e &= \frac{2V}{N(N-1)l_0^2} \cdot \frac{3E}{(1-2\nu)} \\
\lambda &= \frac{V}{N(N-1)(N-2)} \cdot \frac{9E(1-4\nu)}{2(1+\nu)(1-2\nu)}
\end{aligned}
\tag{6}
$$

where V is the volume of a unit cell, and the failure bond strain is calibrated as:

$$
\tilde{\varepsilon}_f = \begin{cases} (1-\alpha)(\tilde{\varepsilon}_b - \tilde{\varepsilon}_y) + \gamma/N \cdot \frac{2G_F V^{1/2}}{f_b l_0} & \text{for 2D - Case} \\ (1-\alpha)(\tilde{\varepsilon}_b - \tilde{\varepsilon}_y) + \gamma/N \cdot \frac{2G_F V^{2/3}}{f_b l_0} & \text{for 3D - Case} \end{cases}
\tag{7}
$$

where the ratio γ/N is related to the specific topology of a unit cell. According to Zhang et al. [39], $\gamma/N \approx 0.33$ for the 2D irregular triangular and $\gamma/N \approx 0.15$ for the 3D irregular tetrahedral cells. As for the other derivatives, e.g. $\partial l/\partial u_i$, $\partial \theta_{IJ}/\partial u_i$, refers to Zhang and Chen [36].
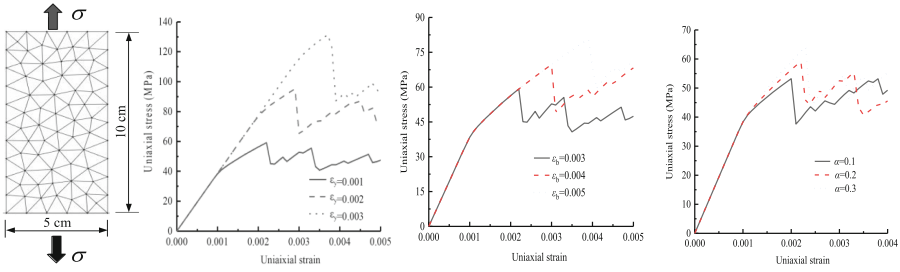
Fig. 2. Parameter sensitivity analysis, (a) simulation specimen; (b) influence of $\tilde{\varepsilon}_y$, $\tilde{\varepsilon}_b = \tilde{\varepsilon}_y + 2 \times 10^{-3}$, $\alpha = 0.2$; (c) influence of $\tilde{\varepsilon}_b$, $\tilde{\varepsilon}_y = 1 \times 10^{-3}$, $\alpha = 0.2$; (d) influence of $\alpha \tilde{\varepsilon}_y = 1 \times 10^{-3}$, $\tilde{\varepsilon}_b = 3 \times 10^{-3}$

3.1 Numerical Implementation

When the numerical simulation is performed by using the SW-DVIB method, the first step is to mesh the object. Usually, the triangular cell (2D problem) or the tetrahedral cell (3D problem) is used. The cell nodal force and cell stiffness matrix can be obtained using a method specified in [27]. The matrices are then combined to form the total nodal force matrix and the total stiffness matrix. The final equilibrium equation can be written into the following matrix form.

$$\mathbf{M}\ddot{\mathbf{u}} + \mathbf{C}\dot{\mathbf{u}} + \mathbf{F}(\mathbf{u}, t) = \mathbf{R}(t) \tag{8}$$

where $\mathbf{M}$ is the lumped mass matrix; $\mathbf{C}$ is the damping matrix; $\mathbf{F}(\mathbf{u}, t)$ is the restoring force vector; $\mathbf{u}$ is the vector of nodal displacement; $\mathbf{R}(t)$ is the external force vector.

3.2 Sensitivity Analysis of the SW-DVIB Method

In order to investigate the influence of micro bond parameters on macro mechanical response of material, a uniaxial tensile case is simulated by the SW-DVIB model. The 2D simulation specimen is shown in Fig. 2a, whose size is 5 cm × 10 cm and the 3-node triangular cell is adopted. The elastic tangent modulus $E = 30$ GPa.

The micro parameter α can influence the macro plastic-elastic ratio of material. The lager the α is, the higher the macro elastoplastic ratio of material is. The simulated result shows the relationship between the micro bond parameters and macro mechanical property of material, which provide meaningful reference for calibration of micro bond parameters.

3.3 Fracture Energy Conservation

In this method, the fracture energy is considered in fracture simulation to make the simulation results independent of the mesh size. To verify the effect of fracture energy, three-point-bending test are simulated by the two methods with and without considering fracture energy. The specimen size and meshing scheme are shown in Fig. 3.
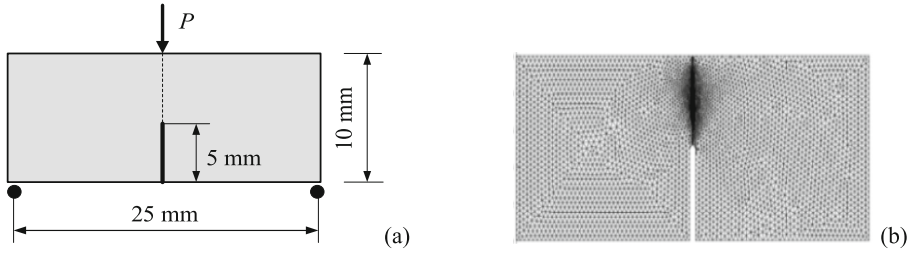
Fig. 3. Three-point-bending test specimen and meshing scheme (a) specimen size; (b) middle mesh

In Case I, the fracture energy is not considered by the setting $\tilde{\varepsilon}_f = \tilde{\varepsilon}_b$. The input micro bond parameters are $E = 42.41 \quad GPa, \tilde{\varepsilon}_y = 1 \times 10^{-3}, \tilde{\varepsilon}_b = 2 \times 10^{-3}, \alpha = 0.2, \upsilon = 0.2, \rho = 2700 kg/m^3$. In Case II, the micro bond parameters are all the same as in Case-I except for the added parameter, fracture energy $G_f = 45$ N/ m. The simulated load-displacement relationship of the loading point is shown in Fig. 4.

In addition to eliminating the mesh-dependence of the force-displacement curve of the loading point, the fracture energy can also eliminate the mesh-dependence of the simulated fracture morphology. For Case-I, due to the fracture energy is not considered, the fracture criterion of microscopic bonds is a prescribed bond length or bond force. Once the bond length or bond force reach the fracture criterion, this bond will break. In this case shown in Fig. 5b-d, with the decrease of element size, the fracture morphology is rougher. However, when fracture energy is considered in Case-II, the fracture criterion of microscopic bonds is related to fracture energy. In this Case, as shown in Fig. 5, the fracture morphology is independent of the element size.
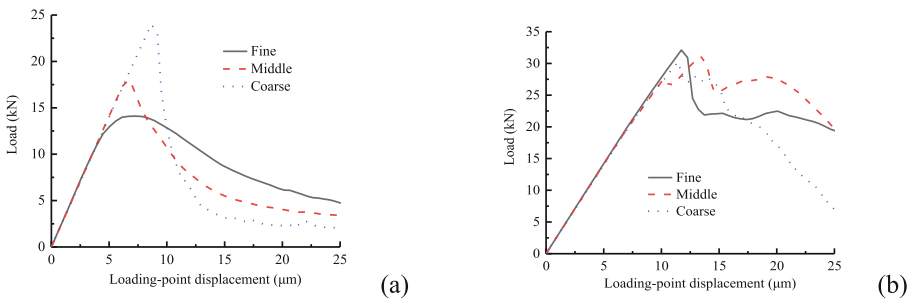

Fig. 4. Simulated load-displacement relation of loading point by the methods of (a) not considering fracture energy; (b) considering fracture energy
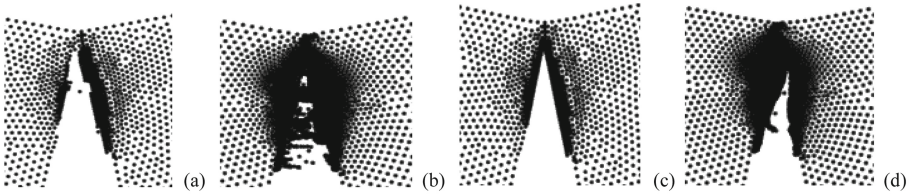
Fig. 5. Simulated fracture morphology by the method; a) Case I: without considering fracture energy for coarse mesh; b) without considering fracture energy for fine mesh, c) with considering fracture energy for coarse; d) Case II: with consideration of fracture energy for fine mesh
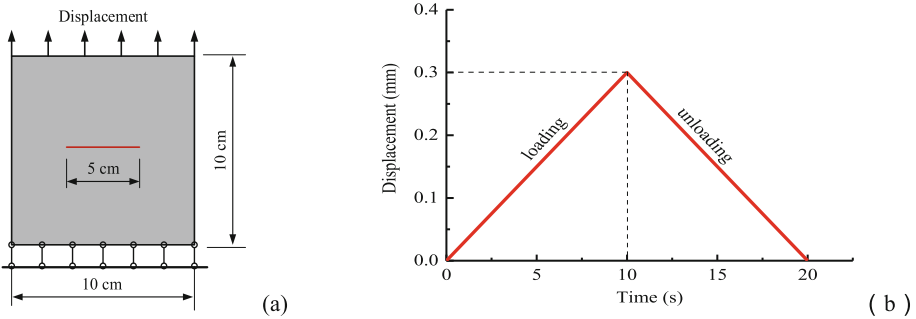

Fig. 6. Loading process of the case of the square plate with a pre-crack (a) model diagram; (b) displacement loading path

4   Simulation Examples

4.1   Elastoplastic Deformation Case

To check the performance of the present method in simulating elastoplastic deformation, we simulate a square plate with a pre-crack. As shown in Fig. 6a, the size of simulation specimen is 10 cm × 10 cm, and there is a pre-crack in the center of the specimen, whose length is 5 cm. The 3-node triangular cell is adopted. There are 25654 triangular cells in the specimen. The displacement loading path is shown in Fig. 6b, the first ten seconds are the loading phase, and the tenth to twentieth seconds are the unloading phase. The input micro bond parameters are $E = 40$ $GPa, \tilde{\varepsilon}_y = 1 \times 10^{-3}, \alpha = 0.2, \rho = 2400\text{kg/m}^3$ (Fig. 7).

4.2   Elastoplastic Fracture Simulation

A uniaxial tensile test of rock specimens with a pre-crack [35] is simulated to study the model's applicability in simulating material fracture. The simplified rock specimen is shown in Fig. 8; the test aimed to investigate the influence of pre-crack dip angle on the material's failure behavior. The following input micro parameters are validated $E = 5.17$ $GPa, \tilde{\varepsilon}_y = 5.1 \times 10^{-4}, \tilde{\varepsilon}_b = 8.67 \times 10^{-4}, \upsilon = 0.2, \rho = 2700\text{kg/m}^3$ (Fig. 9):
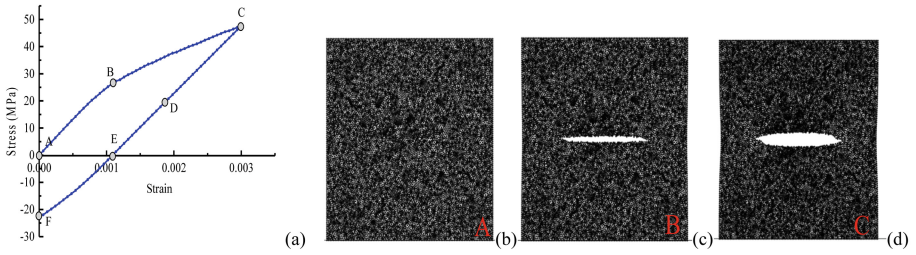
Fig. 7. Simulated deformation process (a) stress-strain relationship; crack opening deformation at (b) $\varepsilon = 0, t = 0$ s; (c) $\varepsilon = 0.00108, t = 4$ s; (d) $\varepsilon = 0.003, t = 10$ s
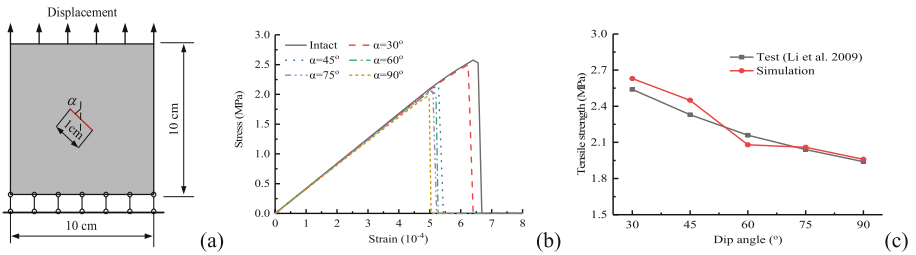

Fig. 8. Model diagram of the uniaxial tension of rock specimen with a pre-crack (a). Simulated results for cases with different pre-crack dip angles (b) stress-strain curves; (c) peak stresses

The simulation examples suggest that the present method can be used to simulate the fracture behaviors of the material

The simulated results shown that the fracture mechanism of specimens with pre-cracks is mainly tensile fracture under uniaxial tensile load. With the change of the pre-crack dip angle, the crack propagation process is basically similar, but the propagation trajectory is different. When $\alpha = 30°$ and $\alpha = 45°$, the initial crack propagation direction has a small deflection from the horizontal direction. When $\alpha = 90°$, the initial crack propagation direction is consistent with the horizontal direction. The comparison between the simulated fracture status and the experimental results [41] is shown.
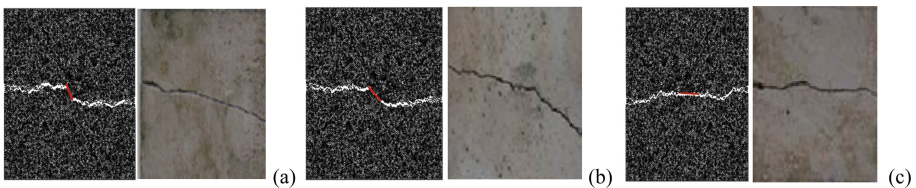

Fig. 9. Comparison between simulated fracture status and experimental results [40] (a)$\alpha = 30°$; (b)$\alpha = 45°$;(c)$\alpha = 90°$. (The left is the simulated result, and the right is experimental)

5   Conclusion

This paper presented the elastoplastic SW-DVIB method for numerical simulation of elastoplastic materials and its application to dynamic fracture propagation in rock. The examples showed that the linear elastic potential SW-DVIB embedded could effectively simulate the fracture damage of elastoplastic materials, and the simulation results do not have the problem of cell size sensitivity, which provides a new solution to the problem of cell size sensitivity. In the simulation example of the dynamic fracture propagation, it was demonstrated that the fracture energy acts an essential role in the propagation of dynamic cracks. The models consider that the energy consumed by the crack propagation of the elastoplastic material is separated into two parts, the first part is used to produce plastic deformation, and the second part is used for fracture failure. By embedding the plasticity into the two-body potential of SW, the SW-DVIB can account for the plastic deformation. Compared with the plastic DVIB developed by Ding, the SW-DVIB can represent the variable Poisson ratio. The simulation results demonstrated that the SW-DVIB could reproduce the loading-unloading plastic behaviors of material. The SW-DVIB promises an approach to simulate plastic fracture propagation.

References

1. Tadmor, E.B, "The quasicontinuum method.," *PhD thesis. Brown University*, 1996.
2. W. A. Curtin and R. E. Miller, "Atomistic/continuum coupling in computational materials science," *Modelling and simulation in materials science and engineering*, vol. 11, no. 3, p. R33, 2003.
3. L. E. Shilkrot, R. E. Miller, and W. A. Curtin, "Multiscale plasticity modeling: coupled atomistics and discrete dislocation mechanics," *Journal of the Mechanics and Physics of Solids*, vol. 52, no. 4, pp. 755–787, 2004.
4. L. E. Shilkrot, W. A. Curtin, and R. E. Miller, "A coupled atomistic/continuum model of defects in solids," *Journal of the Mechanics and Physics of Solids*, vol. 50, no. 10, pp. 2085–2106, 2002.
5. J. R. Rudd, L. M. Barnett, M. L. Butson, D. Farrow, J. Berry, and R. C. Polman, "Fundamental movement skills are more than run, throw and catch: The role of stability skills," *PloS one*, vol. 10, no. 10, p. e0140224, 2015.
6. G. J. Wagner and W. K. Liu, "Coupling of atomistic and continuum simulations using a bridging scale decomposition," *Journal of Computational Physics*, vol. 190, no. 1, pp. 249–274, 2003.
7. H. S. Park, E. G. Karpov, W. K. Liu, and P. A. Klein, "The bridging scale for two-dimensional atomistic/continuum coupling," *Philosophical magazine*, vol. 85, no. 1, pp. 79–113, 2005.

8. H. Gao and P. Klein, "Numerical simulation of crack growth in an isotropic solid with randomized internal cohesive bonds," *Journal of the Mechanics and Physics of Solids*, vol. 46, no. 2, pp. 187–218, 1998.

9. Z. N. Zhang and X. R. Ge, "Micromechanical consideration of tensile crack behavior based on virtual internal bond in contrast to cohesive stress," *Theoretical and Applied Fracture Mechanics*, vol. 43, no. 3, pp. 342–359, 2005.

10. T. Menouillard and T. Belytschko, "Dynamic fracture with meshfree enriched XFEM," *Acta mechanica*, vol. 213, no. 1–2, pp. 53–69, 2010.

11. T. Belytschko, Y. Y. Lu, L. Gu, and M. Tabbara, "Element-free Galerkin methods for static and dynamic fracture," *International Journal of Solids and Structures*, vol. 32, no. 17–18, pp. 2547–2570, 1995.

12. K. Otsuka and H. Date, "Fracture process zone in concrete tension specimen," *Engineering fracture mechanics*, vol. 65, no. 2–3, pp. 111–131, 2000.

13. T. Belytschko and M. Tabbara, "Dynamic fracture using element-free Galerkin methods," *International Journal for Numerical Methods in Engineering*, vol. 39, no. 6, pp. 923–938, 1996.

14. Kou and Zhou, "Application of element-free method to track crack propagation. Using element-free method," *Chinese Journal of Rock Mechanics and Engineering*, vol. 19, no. 1, pp. 18–23, 2000.

15. M. Ostoja-Starzewski, "Lattice models in micromechanics," *Appl. Mech. Rev.*, vol. 55, no. 1, pp. 35–60, 2002.

16. M. Ostoja-Starzewski, P. Y. Sheng, and K. Alzebdeh, "Spring network models in elasticity and fracture of composites and polycrystals," *Computational Materials Science*, vol. 7, no. 1–2, pp. 82–93, 1996.

17. Kawai, Kawabata, and Kumagai, "A new discrete model for analysis of solid mechanics problems," *Numerical methods in fracture mechanics*, pp. 26–37, 1978.

18. P. A. Cundall and R. D. Hart, "Numerical modelling of discontinua," *Engineering computations*, 1992.

19. Sun Qicheng, "Examen de la dynamique des flux de particules et de ses modèles discrets," *Advances in Mechanics*, vol. 38, no. 1, pp. 87–100, 2008.

20. Juemin, "Numerical manifold method and discontinuous deformation analysis[J]. Chinese Journal of Rock Mechanics and Engineering," *Chinese Journal of Rock Mechanics and Engineering*, vol. 16, no. 3, pp. 279–292, 1997.

21. A. Hrennikoff, "Solution of problems of elasticity by the framework method," 1941.

22. Y. Jenq and S. P. Shah, "Two parameter fracture model for concrete," *Journal of engineering mechanics*, vol. 111, no. 10, pp. 1227–1241, 1985.

23. Z. P. Bažant, M. R. Tabbara, M. T. Kazemi, and G. Pijaudier-Cabot, "Random particle model for fracture of aggregate or fiber composites," *Journal of engineering mechanics*, vol. 116, no. 8, pp. 1686–1705, 1990.

24. B. L. Karihaloo, P. F. Shao, and Q. Z. Xiao, "Lattice modelling of the failure of particle composites," *Engineering Fracture Mechanics*, vol. 70, no. 17, pp. 2385–2406, 2003.

25. G.-F. Zhao, J. Fang, and J. Zhao, "A 3D distinct lattice spring model for elasticity and dynamic failure," *International Journal for Numerical and Analytical Methods in Geomechanics*, vol. 35, no. 8, pp. 859–885, 2011.

26. A. Arslan, R. Ince, and B. L. Karihaloo, "Improved lattice model for concrete fracture," *Journal of Engineering Mechanics*, vol. 128, no. 1, pp. 57–65, 2002.

27. A. Wells, "Unstable crack propagation in metals: cleavage and fast fracture," in *Proceedings of the crack propagation symposium*, 1961, vol. 1, no. 84.

28. J. R. Rice, "A path independent integral and the approximate analysis of strain concentration by notches and cracks," 1968.

29. G. Wang, A. Al-Ostaz, A.-D. Cheng, and P. R. Mantena, "Hybrid lattice particle modeling of wave propagation induced fracture of solids," *Computer methods in applied mechanics and engineering*, vol. 199, no. 1–4, pp. 197–209, 2009.
30. Z. Zhang, "Discretized virtual internal bond model for nonlinear elasticity," *International Journal of Solids and Structures*, vol. 50, no. 22–23, pp. 3618–3625, 2013.
31. L. L. Xu, J. B. Cui, S. P. Huang, J. D. Tang, L. Cai, and P. Yu, "Analysis and application of fracture propagated model by hydraulic fracturing in coal-bed methane reservoir," *China Coal Soc*, vol. 39, no. 10, 2014.
32. Zapperi S and Stanley HE, "Plasticity and avalanche behaviour in microfracturing phenomena," *Nature*, vol. 388, pp. 658–60, 1997.
33. Seppala ET and Alava MJ, "Scaling of interfaces in brittle fracture and perfect plasticity," *Phy Rev E*, vol. 61, pp. 6312–9, 2000.
34. Picallo CB, Zapperi S, and Alava MJ, "From brittle to ductile fracture in disordered materials," *Phy Rev Lett*, 2010.
35. J. Ding, Z. Zhang, F. Yang, Y. Zhao, and X. Ge, "Plastic fracture simulation by using discretized virtual internal bond," *Engineering Fracture Mechanics*, vol. 178, pp. 169–183, 2017.
36. Zhang Z and Zheng H, "A modified Stillinger–Weber potential-based hyperelastic constitutive model for nonlinear elasticity," *International Journal of Solids and Structures*, vol. 51.
37. F. H. Stillinger and T. A. Weber, "Computer simulation of local order in condensed phases of silicon," *Physical review B*, vol. 31, no. 8, p. 5262, 1985.
38. Dina Kon, "Modeling Plastic Fracture by Stillinger-Weber Potential-Embedded Discretized Virtual Internal Bond," *International Journal of Scientific Engineering and Research*, vol. 6, no. 12, pp. 2347–3878, 2018.
39. Z. Zhang, Y. Yao, and X. Mao, "Modeling wave propagation induced fracture in rock with correlated lattice bond cell," *International Journal of Rock Mechanics and Mining Sciences*, vol. 78, pp. 262–270, 2015.
40. Li MT, Li SC, and Zhang N, "Influences of 3D internal crack dip angle on tensile mechanical properties and fracture features of rock-like material," *China Journal of Rock Mech Eng*, vol. 28, no. 2, pp. 281–289, 2009.
41. A. Ghazvinian, H. R. Nejati, V. Sarfarazi, and M. R. Hadei, "Mixed mode crack propagation in low brittle rock-like materials," *Arabian Journal of Geosciences*, vol. 6, pp. 4435–4444, 2013.